Enhancement of cloud cover and suppression of nocturnal drizzle in stratocumulus polluted by haze

A. S. Ackerman,[1] O. B. Toon,[2] D. E. Stevens,[3] and J. A. Coakley, Jr.[4]

Abstract. Recent satellite observations indicate a significant decrease of cloud water in ship tracks, in contrast to an ensemble of *in situ* ship-track measurements that show no average change in cloud water relative to the surrounding clouds. We find through large-eddy simulations of stratocumulus that the trend in the satellite data is likely an artifact of sampling only overcast clouds. The simulations instead show cloud cover increasing with droplet concentrations. Our simulations also show that increases in cloud water from drizzle suppression (by increasing droplet concentrations) are favored at night or at extremely low droplet concentrations.

1. Introduction

The effects of aerosols on clouds constitute a major uncertainty in predictions of global climate change [*Houghton et al.*, 2001]. A subset of sufficiently large and wettable aerosols serve as cloud condensation nuclei (CCN) that determine the number concentration of cloud droplets during cloud formation. The primary effect of increased concentrations of CCN is to redistribute cloud water over a greater number of droplets, thereby increasing total droplet cross-sectional area and hence cloud albedo. This effect was first suggested by *Twomey* [1974] as a mechanism by which pollution can exert a strong radiative cooling effect on global surface temperatures. Beyond this so-called "Twomey effect" are possible secondary effects resulting from suppression of precipitation by smaller droplets. These are expected to amplify the negative radiative forcing by increasing cloud water [*Pincus and Baker*, 1994] and cloud cover [*Albrecht*, 1989].

We focus on low-lying stratiform marine clouds because they cover vast areas of the global ocean, reflect much more sunlight than the underlying ocean surface, and do not appreciably affect outgoing thermal radiation. The response of clouds to regional-scale variations in CCN are invariably subject to co-varying meteorological conditions, muddling the cloud microphysical response with changes from dynamical forcings [*e.g., Harshvardhan et al.*, 2002]. To bypass such a tangling of signals, we consider the natural laboratory of ship tracks, which are linear features of enhanced albedo in clouds polluted by ship exhaust [*Conover*, 1966; *Coakley et al.*, 1987], in which the only significant perturbation is the aerosol loading within the exhaust plume.

The primary (or "Twomey") effect is robustly observed in ship tracks [*Durkee et al.*, 2000; *Ackerman et al.*, 2000]. Evidence for secondary effects is ambiguous. Airborne remote sensing of ship tracks during the Monterey Area Ship Tracks (MAST) experiment indicates that cloud liquid water path (LWP) increases in some ship tracks and decreases in others [*Platnick et al.*, 2000]. Similarly, an ensemble of 64 ship track *in situ* interceptions obtained during MAST reveals changes in cloud water (Fig. 1) that are not statistically different from zero on average [*Ackerman et al.*, 2000] (see Appendix A). However, a more recent analysis of hundreds of 30-km segments of ship tracks from 1-km resolution satellite measurements [*Coakley and Walsh*, 2002] surprisingly shows a statistically significant 16% decrease of LWP in ship tracks relative to the surrounding clouds (Fig. 1). Here we use large-eddy simulations with detailed microphysics and radiative transfer to investigate this apparent discrepancy between the satellite and *in situ* measurements. We find that the strong satellite signal is likely an artifact of sampling only overcast pixels.

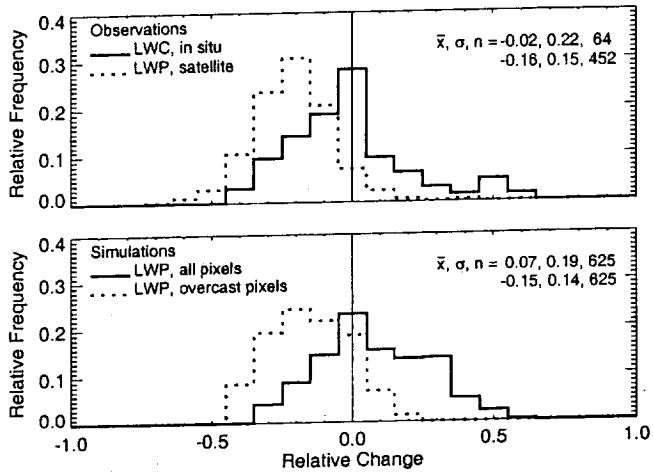

Figure 1. Frequency histograms of changes (relative to background clouds) in liquid water content (LWC) measured *in situ* and liquid water path (LWP) from satellite measurements of ship tracks (top panel) and between model simulations with CCN number concentrations fixed at 75 and 150 cm^{-3} (bottom panel). For comparison with the satellite measurements (obtained around 4 PM local time from 30-km segments of 1 km pixels), the model output are sampled (every 5 minutes) between 3 and 5 PM, and differences taken between domain averages. A 1.1 × 1.1 km pixel is considered overcast in the simulations if the optical depth in 90% of its 256 model columns exceeds 2.5. Mean value, standard deviation, and total number of samples are listed for each distribution.

2. Results

Convection in the stratocumulus-topped marine boundary layer is driven largely by longwave cooling near cloud top [*Lilly*, 1968]. Solar heating offsets some of that cooling and thereby inhibits convection, reducing the supply of moisture from the surface [*Nicholls*,

[1] NASA Ames Research Center, Moffett Field, CA 94035.
[2] University of Colorado, Boulder, CO 80309.
[3] Lawrence Livermore National Laboratory, Livermore, CA 94552.
[4] Oregon State University, Corvallis, OR 97331.

Paper number 2000???000000.
0094-8276/02/2000???00000$5.00

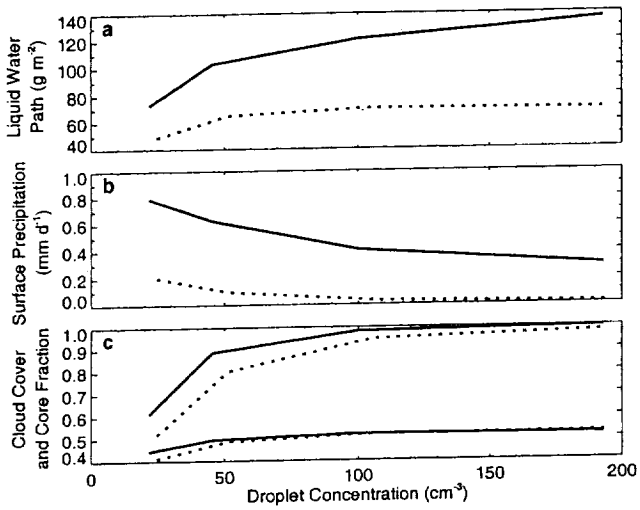

Figure 2. Domain-average properties from nocturnal (solid lines) and daytime (dotted lines) large-eddy simulations of marine stratocumulus with CCN number concentrations fixed at 40, 75, 150, and 300 cm^{-3}. Plotted against the average cloud droplet concentration in cloudy grid cells (those with liquid water mixing ratio > 0.05 g kg^{-1}) are (a) liquid water path, (b) surface precipitation rate, and (c) fractional cloud cover (upper curves, defined as in [*Wyant et al.*, 1997] by the fraction of model columns with optical depth > 2.5). and maximum core fraction (lower curves, where core fraction is defined as in Stevens *et al.* [2001] by the fractional number of cloudy, buoyant grid cells in each model layer). The data are averaged over the last 10 h of 12 h simulations.

1984]. (In our simulations, described in Appendix B, the peak solar heating rate is ~1 K h^{-1} at noon, which is 20% of the peak longwave cooling rate.) As seen in Fig. 2, the more vigorous convection at night enhances LWP in nocturnal simulations relative to the daytime; the enhanced nocturnal LWP increases the surface precipitation flux relative to the daytime; and the enhanced nocturnal convection results in greater cloud cover at night for any given droplet concentration. The response of precipitation to increased droplet concentrations is slight in the daytime simulations: at droplet concentrations > 50 cm^{-3} the drizzle flux in the daytime simulations is already so small that reducing it further has little effect on the average LWP.

The most dramatic changes in LWP with droplet concentrations occur at the lowest droplet concentrations. At the lowest droplet concentrations there is too much drizzle to maintain a radiatively-driven, stratocumulus-topped boundary layer [*Ackerman et al.*, 1993], which is replaced by a field of shallow cumulus [*Stevens et al.*, 1998]. The transition from stratocumulus to shallow cumulus is evident in synthetic images of cloud albedo (Fig. 3). The fractional area of convective cloud cores is ~1/2 in the stratocumulus, but falls below that level in the more cumuliform convection arising at the lowest droplet concentrations (Fig. 2c). The fractional cloud cover approaches that of convective cores at the lowest droplet concentrations, indicating that cloudy air detrained from the convective cores does not extend far from those cores.

The cumuliform convection of the clean boundary layer results from increased atmospheric stability, in which weaker eddies are resisted and vertical mixing is dominated by the strongest eddies. The increased atmospheric stability at reduced droplet concentrations results from more cooling below cloud base by greater drizzle evaporation [*Nicholls*, 1984] and greater drying near cloud top by drizzle formation. The drying diminishes the radiative cooling rate [*Ackerman et al.*, 1993], and decreases the (convectively favorable) latent cooling of cloudy air during descent [*Stevens et al.*, 1998]. However, this cumuliform convection is highly susceptible to changes in aerosol populations, as found in field measurements [*Taylor and Ackerman*, 1999] and model simulations [*Stevens et al.*, 1998].

During extremely clean conditions, the injection of ship exhaust has been observed to rapidly transform shallow, cumuliform clouds in the boundary layer into a prominent cloud line [*Taylor and Ackerman*, 1999]. Visible ship tracks are seen most often in cloud fields that are patchy [*Scorer*, 1987]. Such tracks, however, are not included in satellite observations that are confined to overcast conditions (for both the ship track and the surrounding clouds). Our daytime simulations at a CCN concentration of 75 cm^{-3} (and an average droplet concentration of ~50 cm^{-3}) are more microphysically representative of the satellite background conditions, with comparable cloud droplet effective radii of 13.5 μm for the satellite data and 14.0 μm for the simulated clouds. As the CCN concentration doubles (and average droplet effective radius decreases by 3.1 μm), the domain-average daytime LWP changes little in the simulations (Fig. 2a), in contrast with the 16% average reduction of LWP in ship tracks indicated by the satellite data (Figs. 1 and 4). However, the satellite observations were restricted to overcast pixels, and our simulations indicate that cloud cover increases with CCN concentrations (Figs. 2c and 3).

Omitting clear and partly cloudy pixels artificially enhances the (filtered) LWP of cloud fields, and the magnitude of the enhancement increases with the number of pixels omitted. Hence, given two cloud fields with the same domain-average LWP, the field with

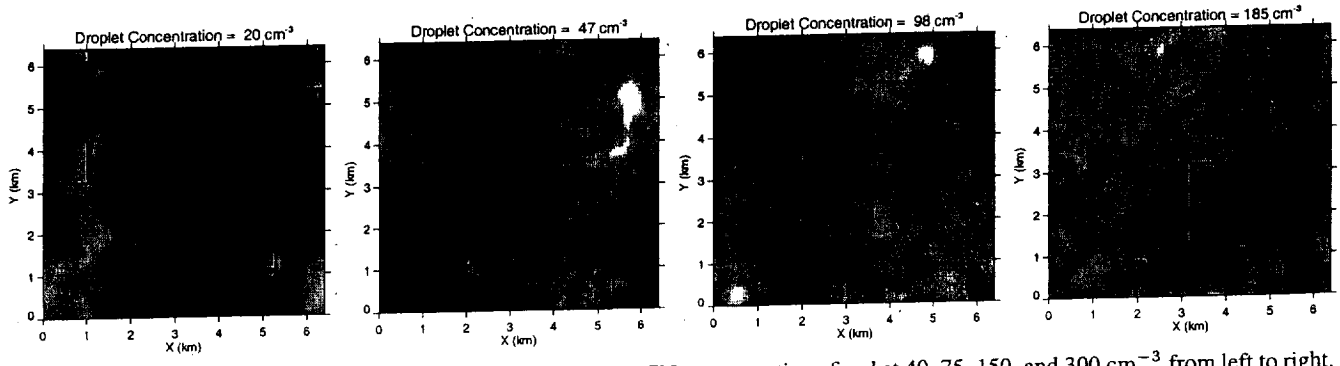

Figure 3. Cloud albedo at 3 PM local time in simulations with CCN concentrations fixed at 40, 75, 150, and 300 cm^{-3} from left to right. The average cloud droplet concentration in cloudy grid cells (as in Fig. 2) for each scene is given. Dark squares outline 1.1 × 1.1 km regions that are < 90% cloudy (defined in Fig. 1).

a broader distribution (or skewed toward lower values) of LWP will have more clear and partly cloudy pixels, and hence a greater enhancement of LWP by filtering. The frequency distributions of daytime LWP narrow (and become less skewed) as droplet concentrations increase in the simulations, as seen in Fig. 4. Filtering out the clear and partly cloudy pixels therefore enhances LWP more at reduced droplet concentrations. Although the domain-average LWP increases moderately as CCN concentrations increase from 75 to 150 cm^{-3}, the filtered LWP decreases, resulting in a distribution of LWP change comparable to the satellite data (Fig. 1).

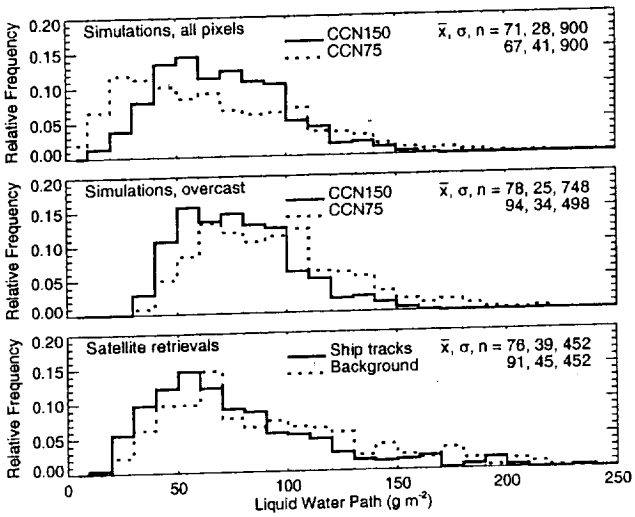

Figure 4. Frequency histograms of liquid water path for all (top panel) and overcast (middle panel, as defined in Fig. 1) 1.1×1.1 km pixels from 3-5 PM in daytime simulations (data output every 5 minutes) with CCN concentrations fixed at 150 and 75 cm^{-3} for the solid and dotted lines, respectively. Bottom panel shows distributions of liquid water path for satellite observations of ship tracks (solid lines) and background clouds (dotted lines). Other notation as in Fig. 1.

3. Discussion

The trend of decreasing breadth of LWP frequency distributions with increasing droplet concentrations is an important (and testable) element in causing the apparent increase of LWP from filtering out all but overcast pixels. As droplet concentrations increase beyond $\sim$50 cm^{-3} the decreasing drizzle flux does not change domain-average daytime LWP appreciably in our simulations, but rather redistributes it spatially. At lower droplet concentrations the fractional area of convective cloud cores increases with droplet concentrations, but this effect diminishes at higher droplet concentrations, as seen in Fig. 2c. With reduced drizzle at higher droplet concentrations, detrained cloudy air persists longer in the clear areas between convective cores, which is the essence of Albrecht's [1989] argument for cloud cover increasing with the lifetime of cloudy air. The visual boundaries of the cloud also encroach on the clear air through the enhanced total droplet cross-sectional area at greater droplet concentrations, which is effectively the Twomey effect applied to detraining cloudy air. (Note that the cloudy elements live longer on the $\sim$1/2 h time scale of a boundary-layer eddy turnover. Our simulations do not address longer time scales relevant to persistence of ship tracks or transitions in cloud regime caused by changing boundary conditions during large-scale, equatorward flow.)

The LWP increase from filtering is greater at lower droplet concentrations because the unfiltered LWP distribution is broader (and more skewed toward zero). However, there is another reason filtering increases LWP more at lower droplet concentrations. Our filter is based on an optical depth cutoff, and optical depth increases with decreasing droplet effective radius. For any given LWP, droplet effective radius decreases and optical depth thereby increases as droplet concentrations increase. Hence, even if the unfiltered LWP distributions were independent of droplet concentration, the filtered LWP would be greater at lower droplet concentrations. This filtering effect is evident in the lower panels of Fig. 4 (for the simulations and satellite data), in which there are fewer samples at low LWP values in the clean distributions compared to their polluted counterparts.

4. Conclusions

We have shown that the *in situ* measurements and satellite retrievals of ship track cloud properties can be reconciled if cloud cover increases with droplet concentrations, as in our simulations. Our analysis suggests that increases in cloud water with increasing droplet concentrations are favored at night or under extremely low droplet concentrations.

Beyond the behavior at extremely low ambient CCN concentrations, in which the ship tracks appear as prominent cloud lines in visible satellite imagery, we expect observable increases of fractional cloud cover in ship tracks arising within more moderate background conditions, with droplet effective radii $< 14\ \mu$m. We also expect the liquid water path in ship tracks to be enhanced relative to surrounding clouds in the morning because of greater drizzle suppression at night.

Appendix A: Filtering of *in situ* Measurements

We omit the five *in situ* penetrations of the *Sanko Peace* ship track, in which the marine boundary layer was observed to rapidly deepen on a day in which extremely low droplet concentrations were recorded in the background clouds [*Taylor and Ackerman*, 1999]. A composited profile of LWC shows LWP increasing significantly in the ship track. Because we bin relative changes in LWC with respect to the background cloud we must omit the data above the background cloud tops where that relative change is infinite. This leaves us to consider the data from flight levels within the background clouds. At those altitudes, drying caused by entrainment of air from above the boundary layer reduced LWC in the ship track. Including only the decrease of LWC measured in those five penetrations would misrepresent the positive LWP change. Hence we omit those five penetrations because they are biased negatively with respect to LWP in the satellite data.

We note that the *in situ* measurements reported by Ackerman *et al.* [2000] are cited by Coakley and Walsh [2002] as evidence supporting the LWP decrease found in their satellite retrievals. However, the cited figure of a 17% decrease is actually the average of the relative change in cloud water divided by the relative change in droplet concentration. The decrease in cloud water itself is much less: if the (biased) *Sanko Peace* data are included (as done by Ackerman *et al.* [2000]), the average relative decrease is only $4 \pm 22\%$.

Appendix B: Description of Model Simulations

The dynamical core of the numerical model is described by Stevens *et al.* [2002] and the cloud microphysics and radiative transfer are described by McFarlane *et al.* [2002]. Here we use a domain

spanning 6.4 × 6.4 km horizontally and 1.5 km vertically, which is discretized into 96 × 96 × 50 equal volume grid cells. A sponge layer at the top of the model dampens trapped buoyancy waves at altitudes > 1250 m. Subsidence and radiative forcings are linearly attenuated to zero in the 300 m above the inversion (defined as the horizontal-average height where the total water mixing ratio exceeds 8.5 g kg^{-1}) to prevent drift of the overlying atmospheric properties resulting from any imbalanced forcings [*Stevens et al.*, 2001]. The particle size distributions are resolved into 20 bins over a range from 0.01 to 4.3 μm radius (bin mid-points) for dry condensation nuclei, which are assumed to consist of ammonium bisulfate, and over a range from 1 to 430 μm radius for activated cloud droplets. The total particle number concentration at each grid point is fixed in each simulation as in McFarlane *et al.* [2002]. The CCN distribution is log-normal with a geometric mean radius of 0.1 μm and a geometric standard deviation of 1.2. Radiative transfer is calculated for each column every 2 minutes. We use Long's [1974] analytic expression to describe droplet gravitational collection efficiencies.

Our simulations are based on an idealization of the First Lagrangian case study from the Atlantic Stratocumulus Transition Experiment [*Duynkerke et al.*, 1995], with model initialization and forcings adapted from the Fourth International Cloud Modeling Workshop (12-16 August 1996, Clermont-Ferrand, France, sponsored by the Global Energy and Water Experiment (GEWEX) Cloud System Studies (GCSS)), also used and described by Stevens *et al.* [1998]. We depart from those specifications by initializing our model domain as initially cloud free (initial relative humidity limited to < 99%) and using surface similarity for surface fluxes, with the sea surface temperature fixed at 290.4 K. Additionally, in place of a parameterized longwave cooling (of up to 74 W m^{-2} in the workshop specification) we use a two-stream radiative transfer model [*Toon et al.*, 1989] in which the water vapor column overlying the model domain is fixed at 1.5 g cm^{-2}, resulting in a net (upward) longwave flux of 80 W m^{-2} above the boundary layer after the cloud layer forms. Solar radiation is calculated for summer solstice at 38° latitude, with time zero corresponding to 6 AM locally.

Daytime simulations for sun angles corresponding to winter solstice resemble our nocturnal results. However, our daytime simulations of stratocumulus at summer solstice are more applicable to their radiative forcing because marine stratocumulus are climatologically favored during the summer off subtropical west coasts, when the marine subtropical highs produce the large-scale meteorological conditions (subsidence and equatorward flow) conducive to extensive stratocumulus decks.

By simply changing CCN concentrations over the entire model domain between simulations, we are not simulating the lateral dispersion of ship tracks, but rather the contrasts between ship tracks and surrounding clouds on scales smaller than the width of mature ship tracks (often > 10 km), representative of regional scale variations in aerosol plumes from larger sources.

Acknowledgments. This work was supported by the Global Aerosol Climatology Project as part of the NASA Radiation Sciences Program.

References

Ackerman, A. S., O. B. Toon, and P. V. Hobbs, Dissipation of marine stratiform clouds and collapse of the marine boundary layer due to the depletion of cloud condensation nuclei by clouds, *Science*, *262*, 226–229, 1993.

Ackerman, A. S., O. B. Toon, J. P. Taylor, D. W. Johnson, P. V. Hobbs, and R. J. Ferek, Effects of aerosols on cloud albedo: Evaluation of twomey's parameterization of cloud susceptibility using measurements of ship tracks, *J. Atmos. Sci.*, *57*, 2684–2695, 2000.

Albrecht, B., Aerosols, cloud microphysics, and fractional cloudiness, *Science*, *245*, 1227–1230, 1989.

Coakley, J. A., Jr, and C. D. Walsh, Limits to the aerosol indirect radiative effect derived from observations of ship tracks, *J. Atmos. Sci.*, *59*, 668–680, 2002.

Coakley, J. A., Jr., R. L. Bernstein, and P. A. Durkee, Effect of ship-stack effluents on cloud reflectivity, *Science*, *237*, 1020–1022, 1987.

Conover, J. H., Anomalous cloud lines, *J. Atmos. Sci.*, *23*, 778–785, 1966.

Durkee, P. A., et al., The impact of ship-produced aerosols on the microstructure and albedo of warm marine stratocumulus clouds: A test of MAST hypotheses 1i and 1ii, *J. Atmos. Sci.*, *57*, 2554–2569, 2000.

Duynkerke, P. G., H. Zhang, and P. J. Jonker, Microphysical and turbulent structure of nocturnal stratocumulus as observed during astex, *J. Atmos. Sci.*, *52*, 2763–2777, 1995.

Harshvardhan, S. E. Schwartz, C. M. Benkovitz, and G. Guo, Aerosol influence on cloud microphysics examined by satellite measurements and chemical transport modeling, *J. Atmos. Sci.*, *59*, 714–725, 2002.

Houghton, J. T., et al. (Eds.), *Climatic Change 2001: The Scientfic Basis*, Cambridge University Press, 2001.

Lilly, D. K., Models of cloud-topped layers under a strong inversion, *Quart. J. Roy. Meteor. Soc.*, *94*, 292–309, 1968.

Long, A. B., Solutions to the droplet collection equation for polynomial kernels, *J. Atmos. Sci.*, *31*, 1040–1052, 1974.

McFarlane, S., F. Evans, and A. S. Ackerman, A Bayesian algorithm for the retrieval of liquid water cloud properties from microwave radiometer and millimeter radar data, *J. Geophys. Res.*, *107*, AAC12–1–21, 2002.

Nicholls, S., The dynamics of stratocumulus: Aircraft observations and comparisons with a mixed layer model, *Quart. J. Roy. Meteor. Soc.*, *110*, 783–820, 1984.

Pincus, R., and M. B. Baker, Effect of precipitation on the albedo susceptibility of clouds in the marine boundary layer, *Nature*, *312*, 250–242, 1994.

Platnick, S., et al., The role of background cloud microphysics in the radiative formation of ship tracks, *J. Atmos. Sci.*, *57*, 2607–2624, 2000.

Scorer, R. S., Ship trails, *Atmos. Environ.*, *21*, 1417–1425, 1987.

Stevens, B., W. R. Cotton, G. Feingold, and C.-H. Moeng, Large-eddy simulations of strongly precipitating, shallow, stratocumulus-topped boundary layers, *J. Atmos. Sci.*, *55*, 3616–3638, 1998.

Stevens, B., et al., Trade-wind cumuli under a strong inversion, *J. Atmos. Sci.*, *58*, 1870–1891, 2001.

Stevens, D. E., A. S. Ackerman, and C. S. Bretherton, Effect of domain size and numerical resolution on the simulation of shallow cumulus convection, *J. Atmos. Sci.*, *0*, In the press, 2002.

Taylor, J. P., and A. S. Ackerman, A case-study of pronounced perturbations to cloud properties and boundary-layer dynamics due to aerosol emissions, *Quart. J. Roy. Meteor. Soc.*, *125*, 2643–2661, 1999.

Toon, O. B., C. P. McKay, T. P. Ackerman, and K. Santhanam, Rapid calculation of radiative heating and photodissociation rates in inhomogeneous multiple scattering atmospheres, *J. Geophys. Res.*, *94*, 16,287–16,301, 1989.

Twomey, S., Pollution and the planetary albedo, *Atmos. Environ.*, *8*, 1251–1256, 1974.

Wyant, M. C., C. S. Bretherton, H. A. Rand, and D. E. Stevens, Numerical simulations and a conceptual model of the stratocumulus to trade cumulus transition, *J. Atmos. Sci.*, *54*, 168–192, 1997.

A. S. Ackerman (corresponding author), NASA Ames Research Center, Moffett Field, CA 94035. (ack@sky.arc.nasa.gov)

O. B. Toon, University of Colorado, Boulder, CO 80309. (btoon@lasp.colorado.edu)

D. E. Stevens, Lawrence Livermore National Laboratory, Livermore, CA 94552. (dstevens@llnl.gov)

J. A. Coakley, Jr., Oregon State University, Corvallis, OR 97331. (coakley@coas.oregonstate.edu)

(Received September 30, 2002.)